

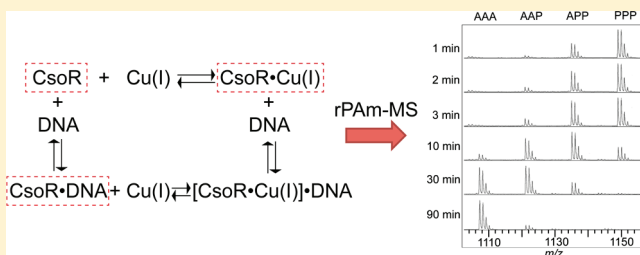
Ratiometric Pulse–Chase Amidination Mass Spectrometry as a Probe of Biomolecular Complex Formation

Feng-Ming James Chang, Matthew A. Lauber, William E. Running, James P. Reilly, and David P. Giedroc*

Department of Chemistry, Indiana University, 800 East Kirkwood Avenue, Bloomington, Indiana 47405-7102, United States

Supporting Information

ABSTRACT: Selective chemical modification of protein side chains coupled with mass spectrometry is often most informative when used to compare residue-specific reactivities in a number of functional states or macromolecular complexes. Herein, we develop ratiometric pulse–chase amidination mass spectrometry (rPAm-MS) as a site-specific probe of lysine reactivities at equilibrium using the Cu(I)-sensing repressor CsoR from *Bacillus subtilis* as a model system. CsoR in various allosteric states was reacted with *S*-methyl thioacetimidate (SMTA) for pulse time, t , and chased with excess of *S*-methyl thiopropionimidate (SMTP) ($\Delta = 14$ amu), quenched and digested with chymotrypsin or Glu-C protease, and peptides were quantified by high-resolution matrix-assisted laser desorption ionization time-of-flight (MALDI-TOF) mass spectrometry and/or liquid chromatography electrospray ionization tandem mass spectrometry (LC–ESI-MS/MS). We show that the reactivities of individual lysines from peptides containing up to three Lys residues are readily quantified using this method. New insights into operator DNA binding and the Cu(I)-mediated structural transition in the tetrameric copper sensor CsoR are also obtained.



Chemical modification has long been used to probe the structure of macromolecules as a function of conformational state, thus providing residue-specific insights into biological function. These techniques are now routinely combined with high-resolution mass spectrometry to monitor the degree of modification by a specific mass shift^{1,2} or sites of intra- or intermolecular cross-linking.^{3,4} Extension of these methods to a ratiometric, pulse–chase approach allows resolution of the intrinsic reactivities of individual side chains toward a modifying agent specifically under equilibrium conditions using isotope- or other mass-encoded labels common in proteomics applications.^{5,6}

Targeting lysine residues is a particularly powerful approach since they are often solvent-exposed and distributed on the protein surface and involved in electrostatic interactions with partner proteins or nucleic acids (DNA or RNA), where they provide substantial stability to protein–protein¹³ and protein–nucleic acid complexes. As a result, lysines are often found at macromolecular interfaces where their reactivities might be expected to be modulated (increased or decreased) as a result of forming various complexes. Previously described radioactivity-based ratiometric pulse–chase methods using trace ³H- and ¹⁴C-acetic anhydride labeling were capable of resolving intrinsic reactivities of individual lysines in small proteins in various ligand-bound states.¹⁴ This method is dependent on far less than stoichiometric labeling in the pulse ($\ll 1$ labeled group per protein), a condition not amenable to mass spectrometry-based approaches that require significant levels of modification to be detected using a ratiometric method. Under these conditions, there is the potential to perturb complex formation since the original charge on the amino groups at neutral pH is rendered

neutral by acetylation and may well suffer from suppressed ionization efficiencies if a peptide does not contain an arginine or a histidine.¹⁵ Other acylation strategies such as succinylation result in the replacement of a positively charged amino group with a negatively charged carboxylate group, which could possibly lead to significant perturbation of the protein structure or complex formation at equilibrium.

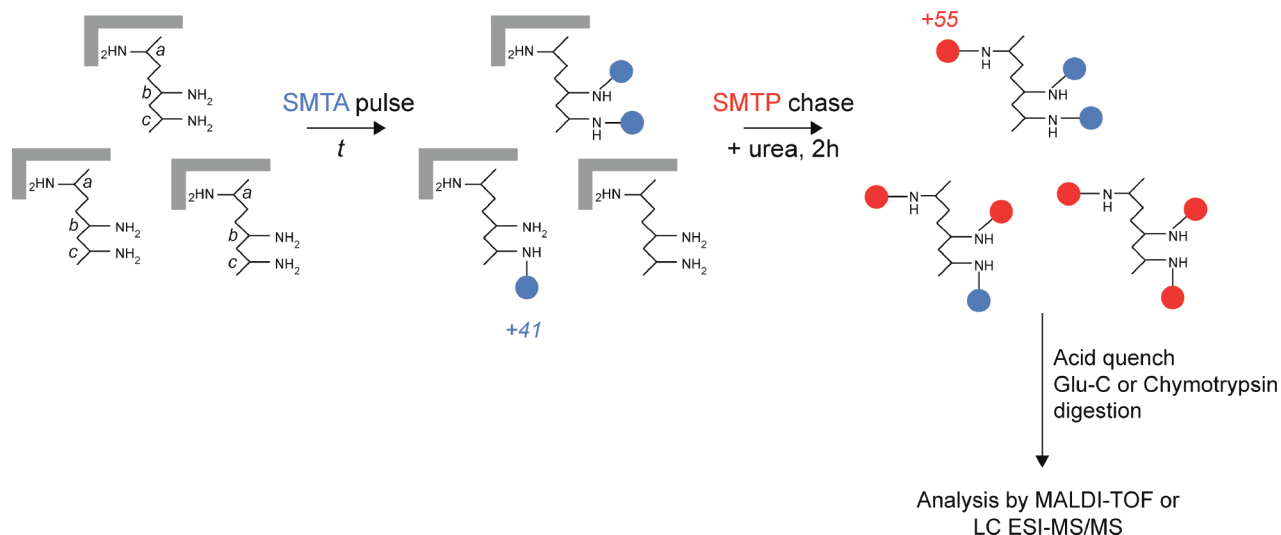
Alkylthioimidates overcome these limitations since they react with primary amines to form protein imines that retain the positive charge of amines at neutral pH and thus exhibit enhanced and predictable ionization efficiencies at acidic pH.^{10,16} Further, amidination may not interfere with biomolecular complex assembly or other functional properties,¹⁷ since electrostatic interactions are intrinsically long-range and often not dependent on the detailed structure of the interaction or ion pair.¹⁸ The approach is amenable to detailed proteomics-based applications¹² and has been used to probe lysine reactivities in large ribonucleoprotein complexes, including the small and large subunits of the bacterial ribosome^{18,19} and protein–ligand interactions in crude protein mixtures.²⁰

In early work, we developed ratiometric pulsed alkylation mass spectrometry (rPA-MS) as a means to probe the reactivities of individual cysteine residues in transition metal coordination complexes formed by metalloregulatory proteins using a pair of differentially isotope-coded *N*-ethylmaleimides.^{7,8} Herein, we outline an analogous approach to specifically probe the reactivities

Received: August 17, 2011

Accepted: October 18, 2011

Published: October 18, 2011

Scheme 1. Schematic Illustration of Ratiometric Pulse–Chase Amidination Mass Spectrometry (rPAm-MS)^a

^a In the first step, primary amines labeled a, b, and c react with a pulse of SMTA (in blue) for a duration of t , following by a chase of SMTP (in red) in a urea-containing buffer. Primary amines are amidated according to their intrinsic reactivity and/or accessibility in the acetamidation pulse phase giving rise to a heterogeneous mixture of molecules; the propionamidation chase reacts with all unreacted lysine residues, the reaction mixture is then acid-quenched, digested by Glu-C protease or chymotrypsin, and the products are analyzed by MALDI-TOF or LC-ESI-MS/MS. Note the Lys residue a is protected from reaction in the pulse due to a direct interaction with a partner macromolecule (gray “L”); other Lys (b, c), while not physically protected by binding react at distinct rates.

of primary amines (α -NH₂, lysine ϵ -NH₂ groups) in proteins termed ratiometric pulse–chase amidination mass spectrometry (rPAm-MS) using companion alkylthioimidates, *S*-methyl thioacetimidate (SMTA) and *S*-methyl thiopropionimidate (SMTP) ($\Delta = 14$ amu),^{9–12} as mass-coded labels.¹⁰ We use this method to probe the reactivities of primary amines using the Cu(I)-sensing repressor CsoR from *Bacillus subtilis* in various allosteric states as a model system.²¹ *Bsu* CsoR is a Cu(I)-sensing repressor that is functionally and likely structurally homologous to the founding CsoR from *Mycobacterium tuberculosis*.^{22,23} Apo-*Bsu* CsoR binds to its GC-rich operator in the *copZA* operon encoding the copper chaperone CopZ and efflux transporter CopA and represses its transcription under conditions of low intracellular Cu.²¹ Under conditions of cytoplasmic Cu(I) stress, CsoR binds Cu(I) which leads to dissociation of CsoR from the operator and transcriptional derepression of *copZA* operon. On the basis of the known structures of CsoR from *M. tuberculosis*²² and *Thermus thermophilus*,²⁴ *Bsu* CsoR is expected to be a D₂ symmetric all α -helical homotetramer (see Supporting Information Figure S3B), experimentally confirmed in the low-micromolar range in the presence and absence of Cu(I).²³ Cu(I) is ligated by Cys45, His70', and Cys74' and shares the same trigonal coordination for Cu(I) as found in *Mtb* CsoR.

The high-resolution structure of *Bsu* CsoR is currently unknown, and very little is known about how CsoR and related CsoR-family tetramers bind their DNA operators;^{26,27} in addition, the structural basis of Cu(I)-induced allosteric switching within the tetramer is only beginning to be understood.²⁵ Here, we develop rPAm-MS to obtain new insights into *Bsu* CsoR structure and regulation.

EXPERIMENTAL SECTION

Pulse–Chase Amidination. The mass-coded amidinating reagents SMTA and SMTP were dissolved in buffer A (250 mM

HEPES, 100 mM NaCl, pH 8.0) and buffer B (250 mM HEPES, 100 mM NaCl, pH 8.0, 6 M urea), respectively, prior to the reaction. Amounts of 400 μ L of samples containing 6 nmol of monomer (15 μ M monomer; 2.5 μ M tetramer) apo-CsoR samples were prepared in 50 mM HEPES, 100 mM NaCl, 2.0 mM dithiothreitol, pH 8.0 for each pulsed amidination experiment. Apo-CsoR (72 nmol or 180 μ M total primary amines) was pulse-amidinated with the addition of SMTA to 0.018 M (7200 nmol; 100-fold molar excess over primary amines). At different pulsed time intervals (t), a 50 μ L aliquot of pulse-amidinated protein was removed and added to 90 μ L of 0.2 M SMTP dissolved in buffer B to a final concentration of 0.13 M in 3.6 M urea (2020-fold molar excess over primary amines) at room temperature for 2 h. The reactions were then quenched by acidification with the addition of 20 μ L of 10% formic acid to a final concentration of 1.25%. The acidified sample was diluted to 400 μ L with 1% formic acid and subjected to two cycles of buffer exchange with 1% formic acid using an Amicon microconcentrator (MW cutoff 3 kDa) 11 500 rpm for 15 min each and then with two cycles of 100 mM NH₄HCO₃. Approximately 50 μ L of each sample was obtained after buffer exchange, and each sample was aliquoted into two separate tubes, one for Glu-C protease digestion and one for chymotrypsin digestion. Amounts of 200 μ g/mL endoproteinase Glu-C or chymotrypsin were then added to an enzyme/substrate ratio \sim 1:50 (w/w) and incubated for 37 $^{\circ}$ C for 18 h. The digested peptides were loaded onto a C18 ZipTip column (Millipore) and eluted with 50% acetonitrile, mixed with CCA matrix at a 5:1 ratio, and 1 μ L was spotted onto a matrix-assisted laser desorption ionization (MALDI) plate and subjected to MALDI time-of-flight (MALDI-TOF) mass spectrometry. The same experiments were also performed with the Cu–CsoR complex and DNA–CsoR complex. For pulse–chase amidination of the DNA–CsoR complex, a 32 bp DNA derived from the *copZA* operator–promoter region (5'-GTTGTAATACCC-TACGGGGGTATGGTAGGATG-3' and the complementary

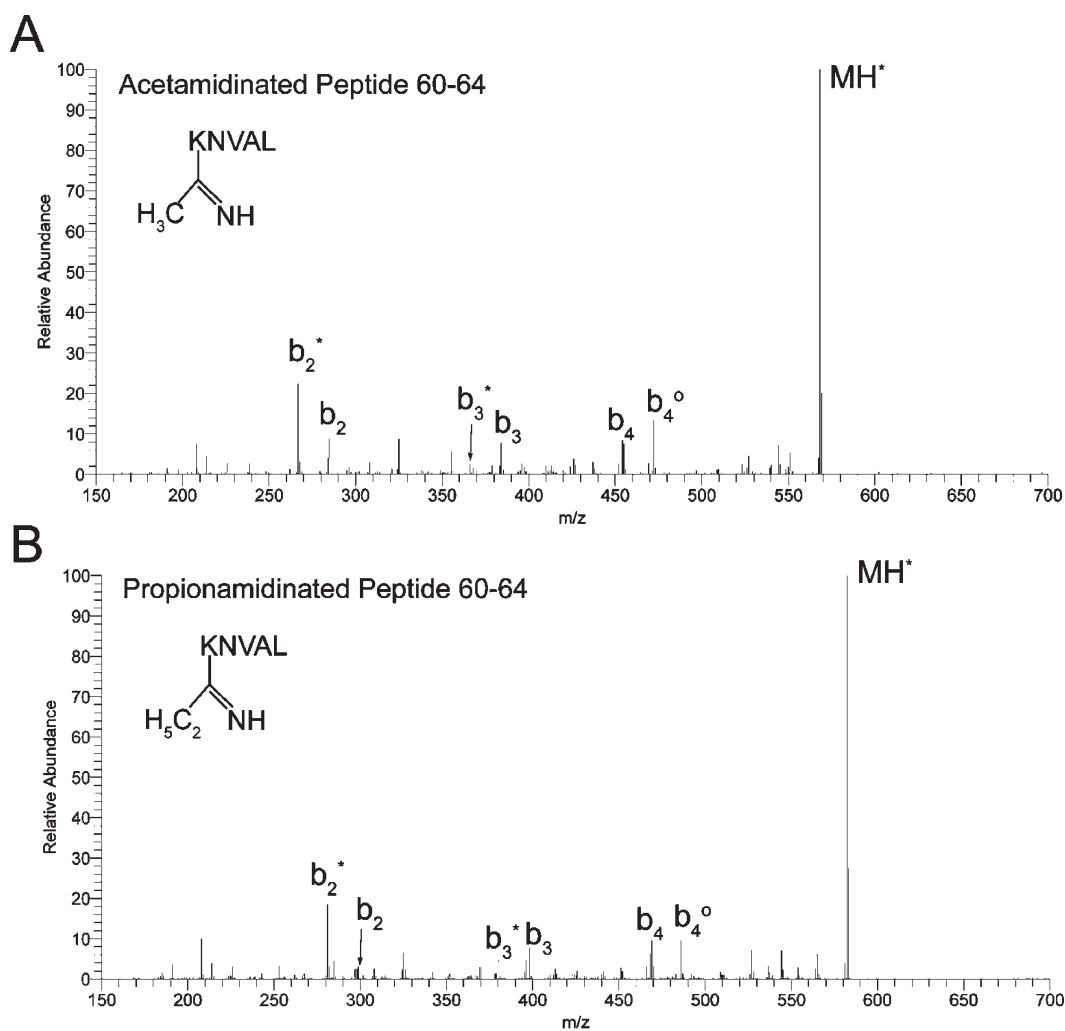


Figure 1. MS/MS spectra of (A) acetamidinated and (B) propionamidinated chymotryptic peptide 60–64. The relative abundances of the corresponding b ions are similar in each peptide. *, deaminated b ion; °, dehydrated during fragmentation.

sequence) was used.²³ To form a DNA–CsoR complex, a sub-stoichiometric amount of six monomer mol equiv of CsoR (15 μ M monomer) was mixed with 2.5 μ M double-stranded DNA to ensure that all protein was bound prior to performing the amidination reaction.

MALDI-TOF Mass Spectrometry. MALDI-TOF mass spectra of all samples were acquired using a Bruker Autoflex III MALDI-TOF mass spectrometer with 200 Hz frequency-tripled Nd:YAG laser (355 nm).

Liquid Chromatography Electrospray Ionization Tandem Mass Spectrometry Analysis of Acetamidinated/Propionamidinated Peptides. See the Supporting Information for details.

RESULTS AND DISCUSSION

Evaluation of Acetamidination and Propionamidination Ionization Efficiencies and Reaction Kinetics. In order to develop the pulse–chase labeling scheme with mass-coded labels SMTA and SMTP outlined in Scheme 1, a necessary condition is that the ability to quantify acetamidinated versus propionamidinated peptides by MALDI-TOF MS versus electrospray ionization tandem mass spectrometry ESI-MS/MS) yields similar results. Previous studies revealed that the ionization efficiencies

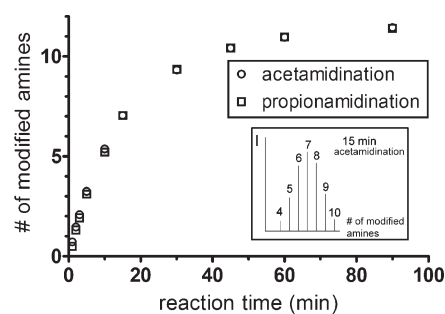


Figure 2. Extent of amidination of apo-CsoR incubated with a 1200-fold excess of SMTA (acetamidination) or SMTP (propionamidination), plotted as the weighted average of derivatized amines as a function of reaction time. A representative determination of weighted average of modified amines is shown in the inset following a 15 min incubation with SMTA. The weighted average of modified amines was calculated from $(\sum i I_i) / \sum I_i$, with I_i being the peak intensity and i being number of modified amines.

of acetamidinated (with SMTA) and propionamidinated (with SMTP) peptides were similar as detected by MALDI-TOF MS¹⁰ and we confirm that here. As shown in Figure 1, MS/MS spectra

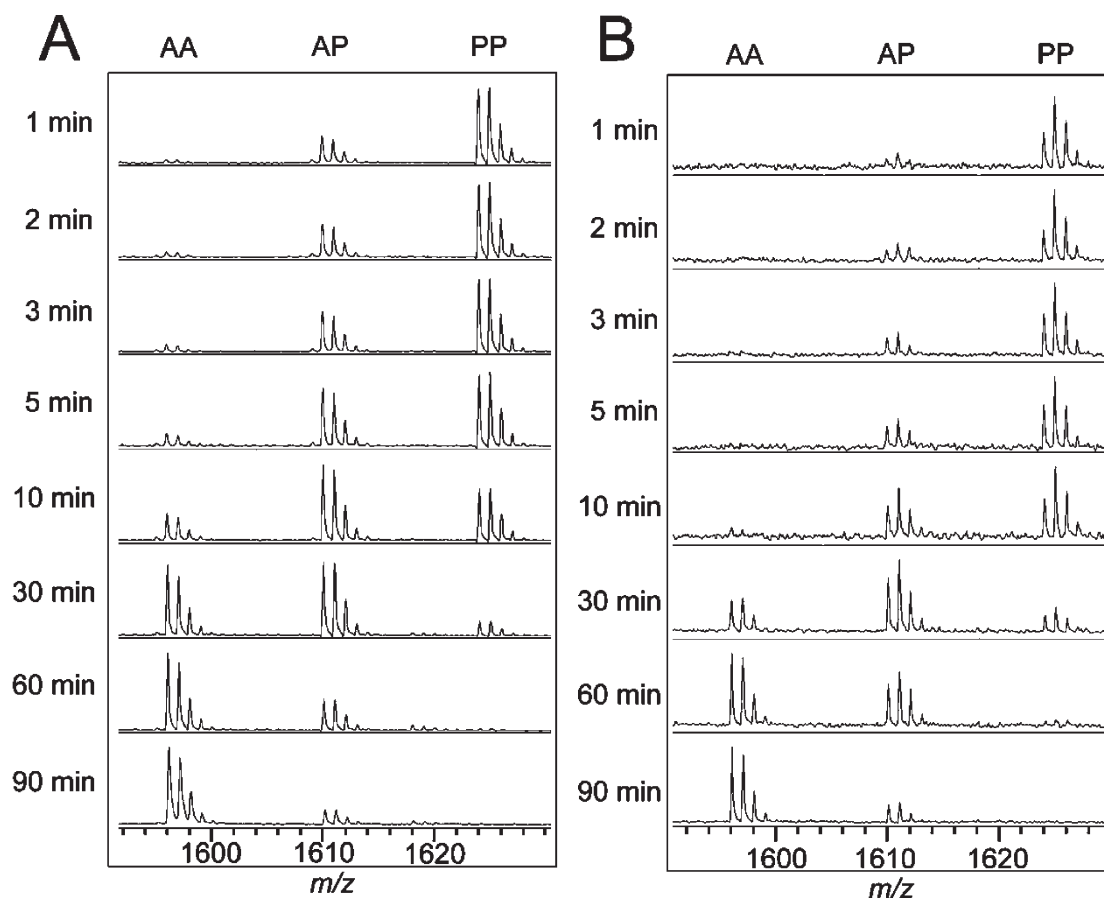


Figure 3. Series of MALDI-TOF mass spectra of peptide 18–29 obtained from a Glu-C protease digest are shown as a function of pulse amidination time t for apo-CsoR (A) and for the apo-CsoR–DNA complex (B). Isotope distribution of three different modified peptides are labeled as AA (doubly acetamidinated), AP (singly acetamidinated/singly propionamidated), and PP (doubly propionamidated) peptides.

of acetamidated versus propionamidated chymotryptic peptide 60–64 are characterized by similar relative peak intensities for directly corresponding b ions (see also ref 12), revealing similar proton affinities in tandem MS/MS, thus establishing a key condition of the method.

Another condition that must be met is that a major fraction of the lysine residues and the α -amino group be quantitatively amidinated and that the reaction kinetics with each reagent were similar or identical. There are 11 Lys residues in *Bsu* CsoR and thus a total of 12 reactive primary amines. In order to obtain amidination reaction kinetics, apo-CsoR was incubated for different times up to 90 min with a 1200-fold excess of SMTA and SMTP, respectively, followed by quenching with 1% formic acid. As shown in Figure 2, the weighted average of amidinated amines calculated from peak intensities measured by ESI-MS was ≈ 11.3 amines after 90 min with both SMTA and SMTP. This reveals that apo-CsoR was nearly quantitatively converted to fully acetamidated or propionamidated protein under these conditions. The kinetics of acetamidation and propionamidation are also essentially identical, thus satisfying a second important condition of the method.

Acetamidated CsoR Retains DNA Binding Activity. In order to determine if the amidination reaction perturbs protein–DNA binding, gel filtration chromatography was used to analyze apo-CsoR–DNA and acetamidated apo-CsoR–DNA complexes. Apo-CsoR or acetamidated apo-CsoR was mixed

with different molar ratios of operator DNA prior to injection into a G200 size exclusion column. As shown in Supporting Information Figure S1, fully acetamidated CsoR recovered at the end of a 90 min incubation with SMTA maintains DNA binding activity, suggesting that acetamidation of primary amines does not significantly alter the CsoR–DNA complex formation.

Overall Acetamidation Reaction Kinetics of CsoR in Three Different Allosteric States. The total extent of acetamidation was compared as a function of time of reaction with SMTA for apo-CsoR, Cu(I)-bound CsoR, and DNA-operator bound CsoR, as shown in Supporting Information Figure S2. Each reaction curve was obtained as described in Figure 2, and the rate constant (k) and extent of labeling (A_{\max}) were determined. A_{\max} for apo-, DNA-bound, and Cu-bound CsoRs were determined to be 10.6 ± 0.2 , 9.0 ± 0.4 , and 9.5 ± 0.2 primary amines, respectively. This reveals that amidination of apo-CsoR bound to the DNA operator occurs with a net recovery of ≈ 2 fewer amidinated lysines over the course of a 90 min reaction, and when all four Cu(I) sites are filled on the tetramer, a net ≈ 1 fewer amidinated groups were recovered on CsoR. Thus, the binding of operator DNA or Cu(I) results in some degree of physical protection from amidination, with DNA binding more effective than Cu(I) binding in this assay.

Ratiometric Pulsed Amidination Mass Spectrometry (rPAM-MS). The pulse–chase amidination experiment (Figure 3) was next performed with these three allosteric states of CsoR in an effort to

Table 1. Amidination Rate Constants for Lysine Residues in Different Allosteric States of CsoR^a

residue ^b	second-order rate constant ($M_{\text{SMTA}}^{-1} \text{ min}^{-1}$) (A_0)		
	apo-CsoR	CsoR–DNA	Cu(I)–CsoR
αNH_2	5.3 ± 0.4 (0.77)	5.8 ± 0.9 (0.96)	ND ^d
K3 ^c	fast: 17.2 ± 5.2 (0.45) slow: 1.3 ± 0.3 (0.55)	1.0 ± 0.1 (0.77)	ND ^d
K18	1.2 ± 0.08 (0.87)	1.1 ± 0.05 (0.94)	0.77 ± 0.03 (0.89)
K26	2.7 ± 0.2 (0.85)	1.8 ± 0.04 (0.94)	3.0 ± 0.1 (0.90)
K60	1.3 ± 0.07 (0.86)	0.85 ± 0.04 (0.83)	1.0 ± 0.05 (0.79)
K80	1.9 ± 0.09 (0.97)	1.8 ± 0.07 (0.97)	2.0 ± 0.1 (0.95)
K96 ^c	7.1 ± 2.3 (0.95) fast: 14.2 ± 5.2 (0.64) slow: 1.7 ± 0.8 (0.36)	2.4 ± 0.3 (0.94) fast: 5.1 ± 2.9 (0.56) slow: 1.3 ± 1.0 (0.44)	4.3 ± 0.6 (0.78) fast: 91 ± 72 (0.26) slow: 4.0 ± 0.6 (0.74)
K97	4.8 ± 0.6 (0.93)	2.4 ± 0.1 (0.85)	4.9 ± 0.5 (0.92)
K100	4.3 ± 0.3 (1.0)	2.0 ± 0.2 (0.88)	4.3 ± 0.3 (1.0)

^a Determined by fitting Θ (P^i) vs pulse time (t) to a single exponential unless otherwise indicated, with the standard error from a representative experiment shown. Amplitude (A_0) is given in parentheses. ^b Quantitative data could not be obtained for peptide 7–17 due to spectral overlap with peptide 91–101. ^c Fit to a sum of two exponentials with A_i (amplitude of the fast and slow phases) indicated in parentheses. ^d ND, not determined. ^e Fits to a single and a sum of two exponentials are shown, with fractional population of each phase given in parentheses.

identify which lysines were protected from modification in the DNA-bound and Cu(I)-bound complexes relative to the apo-CsoR reference state. CsoRs were incubated with SMTA for different pulse times, t , followed by a chase with a large excess of SMTP. The reaction mixtures were then quenched by acidification, the proteins were digested by endoprotease Glu-C or chymotrypsin, and the mole fraction of amidinated (labeled as “A”) versus propionamidinated (labeled as “P”) peptides were determined either by MALDI-TOF or liquid chromatography (LC)–ESI-MS/MS (vide infra). *B. subtilis* CsoR is a challenging experimental target for this method since of the 11 Lys residues (K3, K8, K13, K16, K18, K26, K60, K80, K96, K97, and K100), eight are collectively found in the N-terminal 18 and C-terminal 8 residues and thus are strongly asymmetrically distributed and clustered in the sequence (Supporting Information Figure S3, first entry). Modifications of all 11 lysines and the $\alpha\text{-NH}_2$ group were detected by this method, and quantitative reactivity data could be obtained for 9 of the 12 detected reactive groups (Supporting Information Table S1). Three lysines near the N-terminus, K8, K13, and K16 on Glu-C peptide 7–17 (Supporting Information Table S1), were present in quantities that precluded accurate quantitation due to overlap with Glu-C peptide 91–101 (containing a single missed cleavage) and were therefore not considered further.

Reactivities of K60 and K80 in Different Allosteric States.

Two chymotryptic peptides containing one internal lysine, peptide 60–64 (K60) and peptide 74–92 (K80), were analyzed identically via detection and quantification of mole fraction of acetamidinated (A) and propionamidinated (P) peptides by MALDI-TOF MS (Supporting Information Figures S4 and S5). A representative stack plot of MALDI-TOF spectra for peptide 60–64 in apo- (Supporting Information Figure S4A) and DNA-bound (Supporting Information Figure S4B) CsoR is shown as a function of SMTA pulse time, t . Envelopes of m/z of 585.3 and 599.3 precisely correspond to the expected masses of acetamidinated (A) and propionamidinated (P) peptide 60–64 (Supporting Information Table S1). Integration of the entire isotope distribution of each envelope reveals that (A)-60–64 grows in more slowly in the CsoR–DNA complex relative to apo-CsoR, suggesting some protection of K60 from amidination

when bound to DNA. The pseudo-first-order amidination rate constant, k , is quantified by plotting the mole fraction of propionamidinated K60, $\Theta(P^{K60})$ (see the Supporting Information), from each spectrum for the apo-CsoR (Supporting Information Figure S6A) and CsoR–DNA complex (Supporting Information Figure S6B) as a function of SMTA pulse time t and fitting each data set to a single exponential. The second-order rate constant is obtained by dividing k by the concentration of SMTA in the pulse, and those values in apo-, DNA-bound, and Cu-bound CsoR are 1.3 ± 0.07 , 0.85 ± 0.04 , and $1.0 \pm 0.05 M_{\text{SMTA}}^{-1} \text{ min}^{-1}$, respectively (Table 1). These data are consistent with K60 maximally protected in DNA–CsoR complex and less so in Cu(I)-bound CsoR relative to apo-CsoR.

The identical analysis was performed for chymotryptic peptide 74–92 containing K80, with stacked MALDI-TOF spectra shown in Supporting Information Figure S5 and mole fraction of propionamidinated K80 plotted as a function of pulse time (Supporting Information Figure S6, parts C and D). Second-order rate constants are 1.9 ± 0.09 , 1.8 ± 0.07 , and $2.0 \pm 0.1 M_{\text{SMTA}}^{-1} \text{ min}^{-1}$ in apo-, DNA-bound, and Cu-bound CsoR, respectively (Table 1). These data reveal that unlike K60, K80 exhibits the same chemical reactivity in all three states and is unaffected by ligand binding. Inspection of the homology model reveals that, in the *Bsu* CsoR tetramer, K60 is likely positioned in the middle of the helical bundle and contributes to a region of strong positive electrostatic potential, whereas K80 is located at the loop between $\alpha 2$ and $\alpha 3$ helices in the extreme periphery of the molecule.

Reactivities of K18 and K26 in Different Allosteric States.

Because of the poor sequence coverage and low signal-to-noise ratio obtained for other chymotryptic peptides, we used endoprotease Glu-C to digest CsoR in order to obtain information on the reactivities of the N-terminal and C-terminal lysine residues. As a result, four of the five detected Glu-C peptides with internal lysines contained two or three reactive primary amines (Supporting Information Table S1 and Figure S3B). It was therefore necessary to obtain the mole fraction of A- versus P-derivatized Lys by ESI-MS/MS, rather than by direct inspection of mole fractions of A- versus P-derivatized peptides by MALDI-TOF MS. As shown below, mole fractions calculated in this way

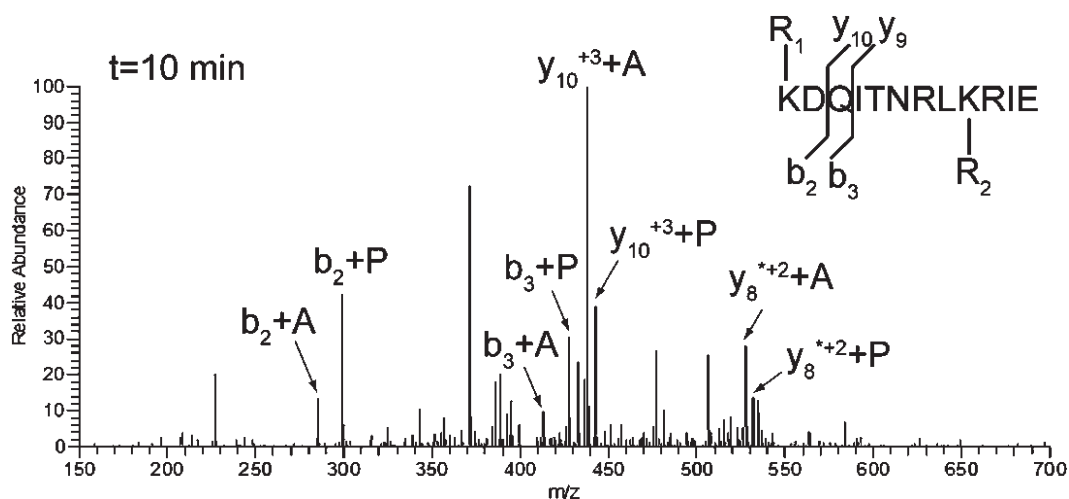


Figure 4. LC-ESI-MS/MS spectrum of peptide 18–29 containing one acetamidated lysine (AP from Figure 3) at pulse time $t = 10$ min. R1 and R2 correspond to acetamidation or propionamidation on the indicated lysine side chain. y and b ions with acetamidated and propionamidated lysine are labeled as +A and +P. Mole ratios of acetamidated and propionamidated lysine corresponding to same b or y ion are calculated directly from the m/z peak intensity. Mean and standard deviation of the mole fraction of $A^{18}P^{26}$ ($\chi(A, P)$) and $P^{18}A^{26}$ ($\chi(P, A)$) are then calculated by averaging the values obtained from different b and y ions (see the Experimental Section).*, deamidated ions detected during the fragmentation process.

quantitatively recapitulate the raw MALDI-TOF MS data (vide infra), consistent with observed similar ionization efficiencies (Figure 1).

Peptide 18–29 is derived from the long $\alpha 1$ helix (Supporting Information Figure S3B) and harbors two lysine residues (K18 and K26). K26 is predicted to form a conserved salt-bridge with K40' on the opposite protomer within the four-helix bundle dimer of dimer architecture of CsoRs (Supporting Information Figure S3B). A stack plot of MALDI-TOF MS for peptide 18–29 in apo- (Figure 3A) and DNA-bound (Figure 3B) CsoRs collected as a function of SMTA pulse time, t , reveals three m/z envelopes of 1595.9, 1610.0, and 1623.9, which correspond to doubly acetamidated (AA), singly acetamidated/singly propionamidated (AP), and doubly propionamidated (PP) peptide 18–29, respectively (Supporting Information Table S1). Compared with apo-CsoR, peptide 18–29 is more protected from amidation in DNA-CsoR since the isotope distribution peak of doubly acetamidated peptide (AA) grows in more slowly in DNA-CsoR (Figure 3).

To quantify the mole fractions of site-specifically A- and P-derivatized K18 and K26, these samples were analyzed by LC-ESI-MS/MS and the fragmentation pattern of the AP peptide for each pulse time t was determined by integration of the MS/MS spectra (Figure 4, $t = 10$ min shown). These data were then quantified and added to that determined by direct integration of the PP and AA peaks from the MALDI-TOF mass spectra (Figure 3) to obtain mole fraction (Θ) A^{K18} , P^{K18} , A^{K26} , and P^{K26} (eqs 6–12, Supporting Information). To determine the rate constant of amidation for each K_i , $\Theta(P^{K_i})$ is plotted as a function of pulse time, t and fit to a single exponential to determine the pseudo-first-order rate constant (Supporting Information Figure S7) with second-order rate constants compiled in Table 1. These data reveal that K26 is about 2.5-fold more reactive than K18 in apo-CsoR and each is differentially affected by ligand binding (Table 1). The reactivity of K18 is insensitive to DNA binding but is attenuated by Cu(I) binding; in contrast, K26 is protected by DNA binding and unaffected by Cu(I) binding to the tetramer.

Partial Deamidation of Peptide 18–29 during Glu-C Digestion. Closer inspection of the MALDI-TOF MS spectra obtained for the peptide 18–29 reveals distinct isotopic distribution patterns for the doubly propionamidated (PP) peptide 18–29 in CsoR–DNA complex (Figure 3B) relative to apo-CsoR (Figure 3A). Theoretical calculations of doubly propionamidated (PP) peptide 18–29 reveal that the second isotopic peak should be 90% as intense as monoisotopic peak, which is not the case for in DNA-CsoR complex spectra (Figure 3B). One likely explanation for this is partial deamidation during the Glu-C digestion, where some amide groups are converted into carboxyl groups leading to a 1 Da increase in mass. To minimize any impact of this, we chose to integrate the entire isotopic distribution in all calculations of peak area rather than the height of monoisotopic peak.

Reactivities of the α -Amino Group and K3 in Different Allosteric States. The reactivities of K3 and the α -NH₂ group were determined from N-terminal peptide 1–6 using exactly the same analysis employed for peptide 18–29. Mole fractions of propionamidated K3 and α -NH₂ were calculated and plotted as a function of pulse time (Supporting Information Figure S8), and rate constants were determined in each allosteric state (Table 1). The reactivity of K3 in apo-CsoR is only consistent with biphasic kinetics, with a burst phase ($A_f = 0.45$) of $k_f = 17.2 \text{ M}_{\text{SMTA}}^{-1} \text{ min}^{-1}$, with the α -NH₂ group defined by a single-exponential decay (Supporting Information Figure S8). Interestingly, the reactivity of K3 is significantly protected in the CsoR–DNA complex, whereas the α -amino group is insensitive to DNA binding.

Reactivities of K96, K97, and K100 in Different Allosteric States. The C-terminal Glu-C peptide 94–101 contains three clustered lysines (K96, K97, and K100) and is predicted to be positioned in or near the central “cavity” that defines the tetramer interface (Supporting Information Figure S3B). As expected, four different m/z envelopes incrementally separated by 14 amu and assignable to AAA, AAP, APP, and PPP were detected in a stack plot of MALDI-TOF mass spectra acquired as a function of SMTA pulse time, t (Supporting Information Figure S9) and are

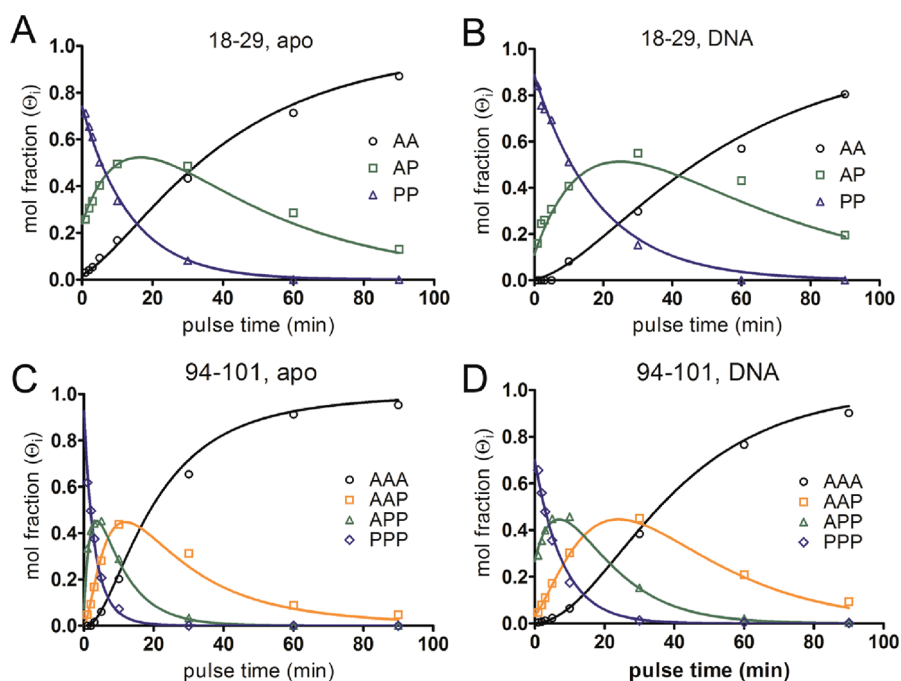


Figure 5. (A and B) Mole fraction of AA-, AP-, and PP-modified peptide 18–29 recapitulated by amidination rate constants of K18 and K26 given in Table 1 (continuous curves) superimposed on experimental data obtained from MALDI-TOF using eqs 3–12 as outlined in the Supporting Information (open symbols). (C and D) Mole fraction of AAA-, AAP-, APP-, and PPP-modified peptide 94–101 obtained from amidination rate constants of K96, K97, and K100 (continuous curves) recapitulates the experimental data obtained directly by MALDI-TOF mass spectrometry (open symbols).

representative of eight different modification states (2^3). In this case, mole fractions of acetamidinated K96, K97, and K100 were readily obtained from integration of the b and y ions of MS/MS spectra of the fragmented AAP and APP ions as a function of pulse time, which when combined with the mole fraction of AAA and PPP peptides from integration of the MALDI-TOF mass spectra gives rise to mole fraction of propionamidinated K96, K97, and K100. These data were then plotted as a function of pulse time t (Supporting Information Figure S10). Unlike the case for peptide 18–29, quantitative analysis of the kinetic data reveals that K96 in apo-CsoR is best fit as a sum of two exponentials with a fast phase rate constant, k_b of $14.2 \text{ M}_{\text{SMTA}}^{-1} \text{ min}^{-1}$ corresponding to 64% of the total; in contrast, K97 and K100 are best fit by single exponentials of similar relative magnitude in k (Supporting Information Figure S10) (see Table 1). One possible explanation for the biphasic kinetics for K96 is that K96, being among the most highly reactive Lys residues, reacts quickly in the burst phase, whereas neighboring K97 and K100 are unmodified; as soon as sufficient amidinated K97 and K100 builds up, the second slower phase dominates the reaction kinetics at K96.

Quantitation of Mass-Coded Labeling by Alkylthioimides by ESI-MS/MS Analysis Recapitulates Direct Integration of the MALDI-TOF Mass Spectra. Amidination rate constants for the α -NH₂ group and eight separate lysine residues in CsoR in three different allosteric states were determined using this combined MALDI-TOF MS–ESI-MS/MS method (Table 1). Using the rate constants obtained from the integration of ESI-MS/MS data for peptides containing two or three lysines (peptides 1–6, 18–29, 94–101), we back-calculated the theoretical species distribution resolvable by MALDI-TOF MS as a function of pulse time and compared those to the experimentally determined species distribution. These comparisons are shown

for peptide 18–29 in the apo- (Figure 5A) and DNA-bound (Figure 5B) states (AA, AP, and PP), and for peptide 94–101 in the apo- (Figure 5C) and DNA-bound (Figure 5D) states (AAA, AAP, APP, PPP). The agreement between theoretical and experimentally acquired MALDI-TOF spectra is excellent. Thus, mole fractions determined by ESI-MS/MS and MALDI-TOF MS are fully internally consistent, which speaks to the robustness of the analytical method outlined here.

CONCLUSIONS

In this work, we outline a general method to quantitatively probe biomolecular complex formation using a simple, high-sensitivity pulse–chase amidination scheme to measure how the reactivities and/or accessibilities of individual lysines toward an exogenous electrophilic imidate differ in distinct conformational states. rPAm-MS can be considered a companion method to ratiometric pulsed alkylation (rPA-MS) of cysteine residues in proteins described earlier⁸ but may well be of broader utility given the ubiquitous presence of Lys residues in protein–nucleic acid and protein–protein interfaces. Although we have used the method to probe protein–DNA complex formation and protein–Cu(I) binding in CsoR, we anticipate that this method will have significant utility in probing the kinetics of assembly of multiprotein or ribonucleoprotein complexes or by characterizing stable subcomplexes that form along an assembly coordinate at equilibrium^{28,29} and, thus, is complementary to recently described irreversible high-resolution cross-linking methods.^{3,30–32}

These data also provide significant new insights into how apo-CsoR forms a repressing complex under conditions of low Cu(I), as well as the nature of the Cu(I)-induced transition within the tetramer, all in the absence of high-resolution crystallographic structures of any conformational state. Previous work shows that

apo-CsoR and related CsoR-family proteins form 2:1 tetramer/DNA complexes to a single GC-rich 11–12 bp sequence,²⁷ with a prominent patch of positive electrostatic potential on the $\alpha 1$ – $\alpha 2$ helical face, anchored by invariant R15 (R24 in *Bsu* CsoR) and R52 (next to K60 in *Bsu* CsoR) in *Mtb* CsoR,²² and near the Cu(I) binding site (Supporting Information Figure S3A). The data reported here are consistent with a model in which the basic C-terminal “tail” in *Bsu* CsoR combines with this central patch (K60) and N-terminal “tail” region of the $\alpha 1$ helix (K3) to create a continuous surface of positive electrostatic potential across one face of the tetramer, from northwest to southeast in the orientation shown in Supporting Information Figure S3B. K3 and K96 are the most reactive lysines in the apoprotein, and each is characterized by a significant burst phase of modification ($\geq 14 M_{\text{SMTTP}}^{-1} \text{min}^{-1}$), with the reactivity of K96 most strongly attenuated in the CsoR–DNA complex. Interestingly, K96 corresponds to K92 in apo *T. thermophilus* CsoR, where it appears to make an ion pairing interaction across the tetramer interface, and is thus consistent with its high solvent accessibility and reactivity (Table 1) and subsequent protection on DNA binding. In fact, all three C-terminal Lys in the central “cavity” of the tetramer interface (K96, K97, and K100) (Supporting Information Figure S9B) are protected from amidination to approximately the same degree in the DNA-bound complex (Table 1), consistent with a global protection of these residues upon DNA binding by the tetramer (see Supporting Information Figure S11 for a model).

In striking contrast, only two Lys residues, the poorly reactive K18 at the N-terminus of the $\alpha 1$ helix and highly reactive K96 just C-terminal to the $\alpha 3$ helix, are measurably protected from amidination in the Cu(I)-loaded tetramer versus apo-CsoR, and this effect is rather small; other Lys are unaffected by Cu(I) binding. K18 corresponds to R10 in *Mtb* CsoR²² and R13 in *Tth* CsoR²⁴ structures and may be reporting on a repacking of the $\alpha 1$ – $\alpha 2$ interface at the periphery of the bundle which occurs on Cu(I) binding such that the reactivity of K18 is attenuated relative the apo state. Helical repacking appears to characterize the interaction of Ni(II) with CnrX, a membrane-bound Ni(II)/Co(II) regulatory protein that harbors a cytoplasmic helical bundle architecture reminiscent of CsoRs.³³ Likewise, modest protection of K96 may well be reporting on a change in the structure or remodeling of the tetramer interface, which must occur in order to drive allosteric inhibition of operator DNA binding by Cu(I).^{23,25} Further structural and hydrodynamic studies of *Bsu* CsoR in various conformational states are required to extend insights into CsoR function obtained here.

■ ASSOCIATED CONTENT

Supporting Information. Additional information as noted in text. This material is available free of charge via the Internet at <http://pubs.acs.org>.

■ AUTHOR INFORMATION

Corresponding Author

*E-mail: giedroc@indiana.edu.

■ ACKNOWLEDGMENT

We thank Dr. Jon Karty, Director of the Mass Spectrometry Facility, and Dr. Randy Arnold, Director of the Proteomics Laboratory, in the Department of Chemistry, Indiana University for use of their mass spectrometers and initial assistance in

analyzing these data. Helpful discussions with Professor David E. Clemmer are also acknowledged. This work was supported by a Grant from the U.S. National Institutes of Health to D.P.G. (GM042569) and from the U.S. National Science Foundation to J.P.R. (CHE-1012855).

■ REFERENCES

- (1) Przybylski, M.; Kast, J.; Glocker, M. O.; Durr, E.; Bosshard, H. R.; Nock, S.; Sprinzl, M. *Toxicol. Lett.* **1995**, *82–83*, 567–575.
- (2) Przybylski, M. *Adv. Mass Spectrom.* **1995**, *13*, 157–283.
- (3) Petrotchenko, E. V.; Borchers, C. H. *Mass Spectrom. Rev.* **2010**, *29*, 862–876.
- (4) Sinz, A. *Mass Spectrom. Rev.* **2006**, *25*, 663–682.
- (5) Julka, S.; Regnier, F. E. *Briefings Funct. Genomics Proteomics* **2005**, *4*, 158–177.
- (6) Regnier, F. E.; Julka, S. *Proteomics* **2006**, *6*, 3968–3979.
- (7) Apuy, J. L.; Chen, X.; Russell, D. H.; Baldwin, T. O.; Giedroc, D. P. *Biochemistry* **2001**, *40*, 15164–15175.
- (8) Apuy, J. L.; Busenlehner, L. S.; Russell, D. H.; Giedroc, D. P. *Biochemistry* **2004**, *43*, 3824–3834.
- (9) Beardsley, R. L.; Reilly, J. P. *Anal. Chem.* **2002**, *74*, 1884–1890.
- (10) Beardsley, R. L.; Reilly, J. P. *J. Proteome Res.* **2003**, *2*, 15–21.
- (11) Janecki, D. J.; Beardsley, R. L.; Reilly, J. P. *Anal. Chem.* **2005**, *77*, 7274–7281.
- (12) Beardsley, R. L.; Sharon, L. A.; Reilly, J. P. *Anal. Chem.* **2005**, *77*, 6300–6309.
- (13) Banci, L.; Bertini, I.; Ciofi-Baffoni, S.; Del Conte, R.; Gonnelli, L. *Biochemistry* **2003**, *42*, 1939–1949.
- (14) Giedroc, D. P.; Sinha, S. K.; Brew, K.; Puett, D. *J. Biol. Chem.* **1985**, *260*, 13406–13413.
- (15) Chakraborty, A.; Regnier, F. E. *J. Chromatogr. A* **2002**, *949*, 173–184.
- (16) Peters, E. C.; Horn, D. M.; Tully, D. C.; Brock, A. *Rapid Commun. Mass Spectrom.* **2001**, *15*, 2387–2392.
- (17) Liu, X.; Broshears, W. C.; Reilly, J. P. *Anal. Biochem.* **2007**, *367*, 13–19.
- (18) Beardsley, R. L.; Running, W. E.; Reilly, J. P. *J. Proteome Res.* **2006**, *5*, 2935–2946.
- (19) Lauber, M. A.; Running, W. E.; Reilly, J. P. *J. Proteome Res.* **2009**, *8*, 4193–4206.
- (20) Xu, Y.; Falk, I. N.; Hallen, M. A.; Fitzgerald, M. C. *Anal. Chem.* **2011**, *83*, 3555–3562.
- (21) Smaldone, G. T.; Helmann, J. D. *Microbiology* **2007**, *153*, 4123–4128.
- (22) Liu, T.; Ramesh, A.; Ma, Z.; Ward, S. K.; Zhang, L.; George, G. N.; Talaat, A. M.; Sacchettini, J. C.; Giedroc, D. P. *Nat. Chem. Biol.* **2007**, *3*, 60–68.
- (23) Ma, Z.; Cowart, D. M.; Scott, R. A.; Giedroc, D. P. *Biochemistry* **2009**, *48*, 3325–3334.
- (24) Sakamoto, K.; Agari, Y.; Agari, K.; Kuramitsu, S.; Shinkai, A. *Microbiology* **2010**, *156*, 1993–2005.
- (25) Ma, Z.; Cowart, D. M.; Ward, B. P.; Arnold, R. J.; DiMarchi, R. D.; Zhang, L.; George, G. N.; Scott, R. A.; Giedroc, D. P. *J. Am. Chem. Soc.* **2009**, *131*, 18044–18045.
- (26) Iwig, J. S.; Chivers, P. T. *J. Mol. Biol.* **2009**, *393*, 514–526.
- (27) Grosseohme, N.; Kehl-Fie, T. E.; Ma, Z.; Adams, K. W.; Cowart, D. M.; Scott, R. A.; Skaar, E. P.; Giedroc, D. P. *J. Biol. Chem.* **2011**, *286*, 13522–13531.
- (28) Talkington, M. W.; Siuzdak, G.; Williamson, J. R. *Nature* **2005**, *438*, 628–632.
- (29) Bunner, A. E.; Williamson, J. R. *Methods* **2009**, *49*, 136–141.
- (30) Mealman, T. D.; Bagai, I.; Singh, P.; Goodlett, D. R.; Rensing, C.; Zhou, H.; Wysocki, V. H.; McEvoy, M. M. *Biochemistry* **2011**, *50*, 2559–2566.
- (31) Lauber, M. A.; Reilly, J. P. *Anal. Chem.* **2010**, *82*, 7736–7743.
- (32) Lauber, M. A.; Reilly, J. P. *J. Proteome Res.* **2011**, *10*, 3604–3616.
- (33) Trepreau, J.; Girard, E.; Maillard, A. P.; de Rosny, E.; Petit-Haertlein, I.; Kahn, R.; Coves, J. *J. Mol. Biol.* **2011**, *408*, 766–779.